S. Alsop
A. J. Matchett
Department of Chemical Engineering
School of Science and Technology
University of Teesside
Middlesbrough, Cleveland TS1 3BA, England

J. M. Coulthard
Department of Civil Engineering
School of Science and Technology
University of Teesside
Middlesbrough, Cleveland TS1 3BA, England

Experimental Investigation of Effects of Vibration upon Elastic and Cohesive Properties of Beds of Wet Sand

The transmission of sinusoidal vibrations through beds of cohesive particulate solids was measured. Results were interpreted in terms of a critical state model to predict the elastic swelling constant k, and the cohesive stress C. Factorial experimental design was used to identify significant parameters. Factors that affect k include percent moisture, bulk density, sample size, sample shape, the presence of a supporting membrane, and loading order. Factors that affect C include percent moisture and particle size distribution. Factors affecting k were interpreted in terms of their effects upon bed structure and factors affecting C in terms of an equivalent pore water pressure due to capillary and liquid bridge effects. The critical state model was modified to incorporate general relationships between axial and radial strains. © *1995 John Wiley & Sons, Inc.*

INTRODUCTION

The critical state theory of Schoefield and Wroth (1969) and others describes the behavior of saturated soils in terms of an elastic–plastic deformation model, incorporating a yield surface and flow rules. For plastic compression, deformation follows the λ line:

$$v = v_\lambda - \lambda \ln(p'), \tag{1}$$

where v is the specific volume, m^3/m^3, of a solid or m^3/kg of solid (in this article, units of m^3/kg solid will be used); p' is the effective compressive stress in Pa; λ is the slope of the plastic compression line, the λ line in m^3/kg; and v_λ is the value of v at $p' = 1$ Pa in m^3/kg.

The value of p' in Eq. (1) is divided by a reference value of $p' = 1$ in order to maintain dimensional consistency. p' is given in terms of normal stresses as

$$p' = (\sigma'_1 + \sigma'_2 + \sigma'_3)/3 \tag{2}$$

and

$$\sigma'_i = \sigma_i - u$$

Received May 5, 1994; Accepted May 4, 1995.

Shock and Vibration, Vol. 2, No. 5, pp. 383–392 (1995)
© 1995 by John Wiley & Sons, Inc.
CCC 1070-9622/95/050383-10

where σ_i is the applied normal stress in Pa, and u is the pore water pressure in Pa, for saturated systems. A system is only able to move down a λ line, with compression.

If stress is reduced after compression, then the system dilates along the elastic k line. Systems can move along k lines in both compression and dilation, but during compression, the deformation changes from elastic to plastic where the k line intersects with the λ line. The elastic swelling line constant, k, relates the specific volume of the material to the effective compressive stress, p':

$$v = v_k - k \ln(p'). \tag{3}$$

v_k is the value of v at $p' = 1$ Pa (m^3/kg), and k is the slope of the elastic swelling line (m^3/kg). As in Eq. (1), p' is divided by a reference value of $p' = 1$ to maintain dimensional consistency.

Matchett (1992) proposed the use of the critical state theory of soil mechanics to model the effects of vibration upon beds of particulate material (Schofield and Wroth, 1969). He demonstrated the model with reference to the experimental data of Norman–Gregory and Selig (1985). They investigated the transmission of vibration through beds of coarse, dry sand held in soil mechanics rubber membranes on a vertically vibrating plane (Fig. 1). A top cap mass was placed on the top of each sample and accelerometers monitored acceleration of the base and top cap mass.

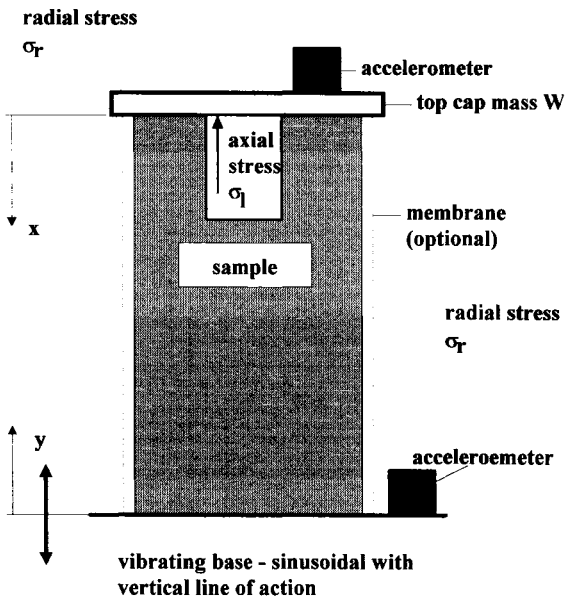

FIGURE 1 Experimental equipment: a triaxial specimen subject to uniaxial vibration.

The elastic, critical state component of the Matchett model, valid for small strains, proposed that the natural frequency of a bed of particulates, a (rad/s), was given by

$$a = 3\sqrt{\frac{p_s v_s}{W k l_s}} \tag{4}$$

where p_s is the static effective compressive stress (Pa); v_s is the static specific volume (m^3/kg); W is the top cap mass (kg/m^2); k is the elastic swelling line constant (m^3/kg); and l_s is the static length of the sample (m).

This article extends this work to a study of cohesive materials and in particular wet sands. When cohesive materials are tested as in Fig. 1, then supporting membranes are no longer needed: the samples are freestanding. Furthermore, the static effective compressive stress, p_s, can be deduced. p_s consists of the effects of top cap mass plus the cohesive stress within the material. If the cohesive stress within the material is C Pa, and C is assumed to be constant through the vibration, then:

$$p_s = \frac{Wg}{3} + C. \tag{5}$$

Equation (3) can be combined with Eq. (4) to give

$$a^2 = \left(\frac{9v_s}{kl_s}\right)\left\{\frac{g}{3} + \frac{C}{W}\right\}$$

$$Q = \frac{a^2 l_s}{v_s} \tag{6}$$

$$Q = \left(\frac{9}{k}\right)\left\{\frac{g}{3} + \frac{C}{W}\right\}.$$

From Eq. (6), a plot of Q versus $1/W$ gives a straight line from which k and C can be determined.

In this model, C is the compressive, cohesive stress that holds the material together. For the wet sands used in this paper, C is caused primarily by liquid bridge bonding, and it is assumed that C acts uniformly in all directions, a reasonable assumption for such a mechanism. The use of C in this context should not be confused with the intercept of a shear stressed–normal stress plot from Jenike cell data. In the context of critical state theory, C can be interpreted as a negative equivalent pore water pressure.

Experimental data collected for wet sands are presented, using the system shown in Fig. 1. The experiments reported have been designed on a factorial basis to investigate those parameters that affect the properties of vibrating beds, when interpreted in terms of the model presented above.

EXPERIMENT PROCEDURE AND DESIGN

These experiments were performed on sand, presieved to three size fractions with size distributions shown in Fig. 2. The sand was dried in an oven at 80°C, and dry sieved to give samples of the required size distribution. Water was mixed with the sand to produce samples of known moisture content, which were left overnight in sealed plastic bags to equilibrate.

The wet sand was made into samples for testing by compression in molds of known sizes to give samples of known densities. The design of the molds enabled the samples to be compressed simultaneously at both ends of the sample, along the axis of major principal stress. Three molds were used as indicated in Table 1.

A sample was placed upon the horizontal base of a sinusoidal vibrator with a vertical line of action, and surmounted by a top cap mass. Accelerometers were mounted on the top cap mass and base (Fig. 1). Tests were performed over a range of frequencies with a constant peak acceleration of 0.08 × g. The magnitude of the acceleration had little effect in the range 0.08–0.15 × g. The accelerometers were of the piezoelectric type and made by Kistler. They were connected, via a coupler, to a CED interface that downloaded the data onto the hard disk of a PC.

Table 1. Details of Molds Used in Experiments

Mold Number	Shape	Size
1	Cylindrical	76 × 38 mm dia.
2	Cylindrical	100 × 50 mm dia.
3	Cube	50 × 50 × 50 mm

The vibrational acceleration of the base and the top cap were measured over a range of frequencies to determine the resonant frequency. The resonant frequency was deemed to be that frequency at which there was maximum amplification between the base and the top cap mass, i.e., the ratio of peak top cap acceleration to peak base acceleration, R, was a maximum. Damped equations were fitted to the R versus frequency data to obtain the best estimate of resonant and natural frequencies, Eqs. (7) and (8). This procedure was repeated for a number of top cap masses in the range 20–200 kg/m^2 for each sample; static axial stresses were in the range 200–2000 Pa.

A series of factorial experiments were designed to determine those factors that have an influence on k and C.

1. Particle size: the sand was taken as received and sieved to <2000, <1000, or <350 μm.

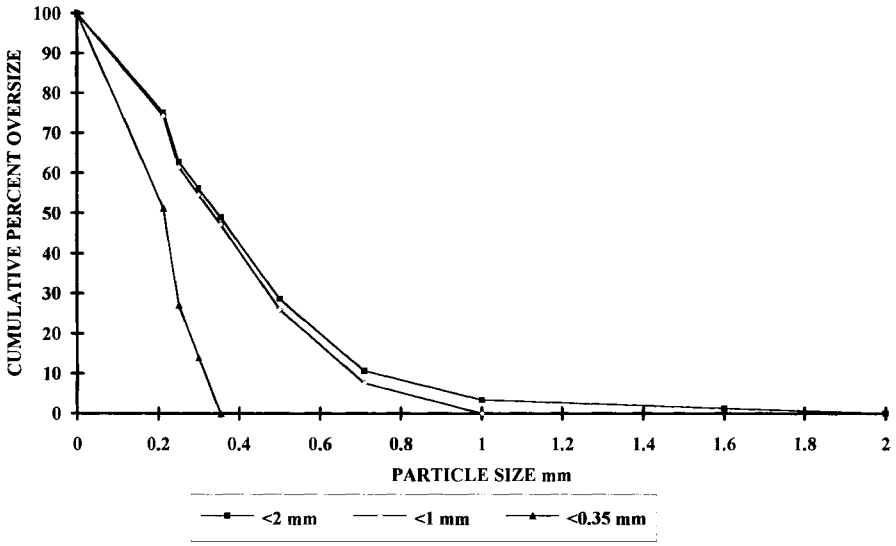

FIGURE 2 Size distribution of the sand fractions used in the tests.

2. Moisture content: two moisture contents were chosen, on a dry weight basis, 3 and 6%.
3. Bulk density: tests were performed at bulk densities of 1500 and 1600 kg/m^3.
4. Sample size: comparison of samples from molds 1 and 2 enabled comparison of samples of the same shape, but different sizes (Table 1).
5. Sample shape: mold 3 is a different shape from molds 1 and 2 (Table 1).
6. Elastic membrane: experiments were performed with membrane enclosed samples and with freestanding samples for mold 1. A standard soil mechanics triaxial testing membrane was used with Young's modulus of 1.12×10^5 Pa.
7. Order of addition of top cap mass: the normal way of performing an experiment was to commence with the lowest value of W and increase top cap mass on the sample as the experiment progressed. A series of tests were also undertaken starting with the maximum value of W and decreasing the mass through the experiment.
8. Sample attitude: the cylindrical samples from molds 1 and 2 were always tested along the axis of major principal stress during formation. With the cubic sample, mold 3, it was possible to perform experiments along the major principle stress axis, and along two axes normal to this axis.

ANALYSIS OF DATA AND RESULTS

The data available from a test consisted of a series of readings of amplification, R, versus driving frequency, w, for each top cap mass W. Typical data are shown in Fig. 3. Data were modeled by a first-order damping mechanism for a spring and damper in series (Thomson, 1981; Matchett, 1992). The acceleration ratio, R, was described by the standard damped oscillation equation:

$$R = \frac{a^2}{\sqrt{(a^2 - w^2)^2 + 4a^2w^2D^2}} \tag{7}$$

with w the driving frequency of the base (rad/s) and D the damping coefficient.

The resonant frequency, a_r, is related to the natural frequency a, as follows:

$$a_r = a\sqrt{1 - 2D^2}. \tag{8}$$

Data of the type shown in Fig. 3 were fitted to Eq. (7) by a least squares procedure from which the least square fit values of a and D were determined, and a_r was calculated from Eq. (8).

The data were then interpreted in terms of Eq. (6), and a^2l/v was plotted against $1/W$. Typical data are shown in Fig. 4.

Data from a block of eight experiments are shown in Table 2 that presents the effects of sample size, percent moisture, and bulk density.

Tables 3 and 4 show the parameters identified

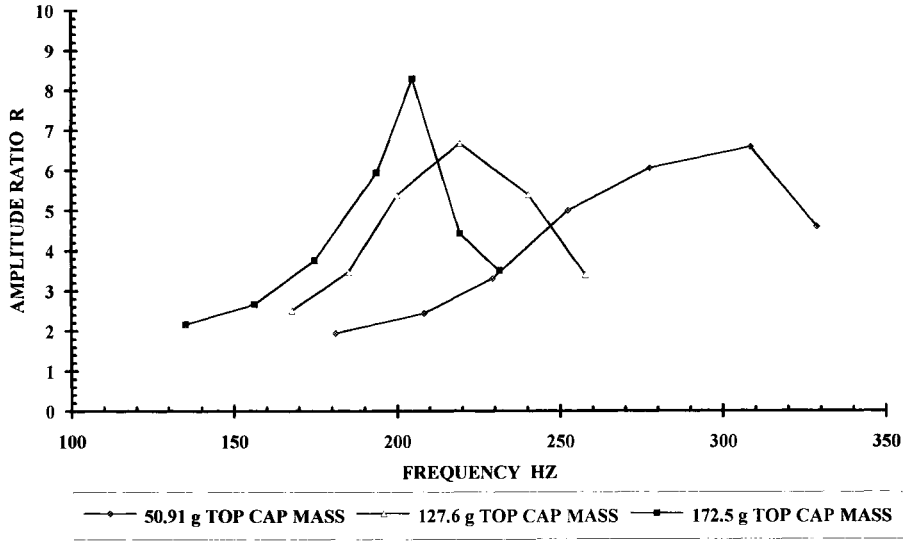

FIGURE 3 Amplification of acceleration R versus frequency: small cylinder 76 * 38 mm; 6.1% moisture; 1500 kg/m^3; particle size <350 μm; no membrane; normal load order.

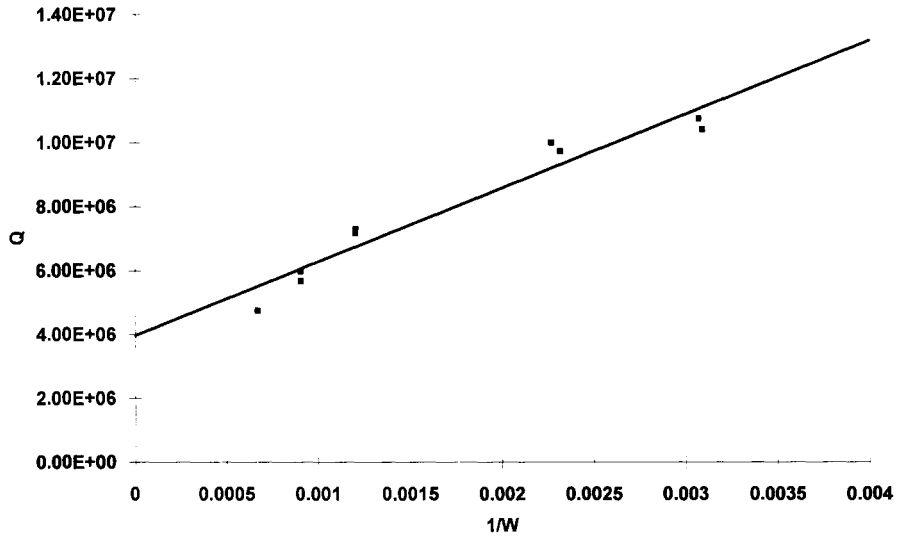

FIGURE 4 a^2 versus $1/W$ for sample as in Fig. 3.

Table 2. k, C, and Correlation Coefficient for Block of Experimental Data

		Small	Mold 1	Large	Mold 2
		(3% H_2))	(6% H_2))	(3% H_2O)	(6% H_2O)
1500	k (m^3/kg)	1.33E-7	2.58E-7	1.76E-7	3.56E-7
kg/m^3	C (Pa)	1006.6	1024.6	971.0	1728.7
	r^2	0.84	0.91	0.88	0.95
1600	k (m^3/kg)	7.96E-8	1.79E-7	1.18E-7	2.06E-7
kg/m^3	C (Pa)	1131.7	1309.6	1289.1	988.4
	r^2	0.92	0.91	0.88	0.74

r^2 is the correlation coefficient for a^2 versus $1/W$ for nine data points. Exponential format has been used for k.

as main effects upon k and C, respectively, along with the direction of action of the parameters.

Values of the damping coefficient D were ~0.08, and thus a and a_r were very close together, Eq. (8). Hence, factorial analysis of data based upon natural frequency and resonant frequency gave similar results. Data presented here are based upon natural frequency.

Table 3. Factors Affecting k: Main Effects

Effect	Level of Significance (%)	Direction
% Moisture	0.01	Positive
Bulk density	0.1	Negative
Particle size (1)	20	—
Particle size (2)	90	—
Sample shape	0.01	Cube > Cylinder
Membrane	1	Membrane > Freestanding
Sample size	2	Positive
Loading order	1	Reverse > Normal
Sample orientation	30	—
Replication	80	—

Particle size (1) compares <2-mm size range with <1-mm size range.
Particle size (2) compares <2-mm size range with <0.35-mm size range.

Table 4. Factors Affecting *C*: Main Effects

Effect	Level of Significance (%)	Direction
% Moisture	2	Positive
Bulk density	90	—
Particle size (1)	15	—
Particle size (2)	1	0.35 > 2
Sample shape	60	—
Membrane	90	—
Sample size	70	—
Loading order	20	—
Sample orientation	90	—
Replication	80	—

Particle size (1) compares <2-mm size range with <1-mm size range. Particle size (2) compares <2-mm size range with <0.35-mm size range.

DISCUSSION

The results will be considered in terms of the critical state model, their practical implications, and as a basis for further investigations.

The critical state model for vibrating solids, Eq. (6), has been successfully applied to damp, cohesive sands. Plots of Q versus $1/W$ give high values of correlation coefficient, significant at the 0.01 level. Values of k and C were calculated (Table 2). This model has also been applied to dry sands by Matchett (1992) using the data of Norman–Gregory and Selig (1985), and therefore, it may have a wide applications potential. Furthermore, replication of experiments is not a significant effect in the data (Tables 3 and 4), suggesting consistency for the experimental technique and the model. However, the experimental method is only applicable over a limited range of applied stresses due to the necessity for the sample to remain freestanding. The stresses used in these experiments, up to 2 kPa, are valid for powder technology applications such as storage of materials in silos. The use in soil mechanics applications at higher stress levels would need to be carefully considered.

The values of k reported in Table 2 and recorded throughout this work are of the order of 10^{-7} m^3/kg or 10^{-4} m^3/m^3. These values are of the order of a factor of 10^{-2}–10^{-3} times those quoted in conventional critical state texts. However, critical state data are quoted for saturated soils, whereas these sands are not saturated, but are held together by the inhibiting effects of liquid bridge bonding. A limited number of control tests on these unsaturated materials in a triaxial tester gave similar values of k to those presented herein.

Damping is small in these systems, as measured by values of D of ~0.08, and this is consistent with other reported work on vibration in soils such as Das (1993).

The effects of parameters on k and C are shown in Tables 3 and 4. These effects will be discussed in terms of a simple analogue shown in Fig. 5, consisting of a spring and a piston. The elasticity of the particle bed is represented by the spring, which is not linear for this critical state model. The cohesive stress is represented by the piston held under vacuum, holding the system together, and the spring under compression. Factors affecting k can be seen as affecting the spring constant, and factors affecting C change the vacuum in the piston. In this context, the critical state swelling line constant, k, is the inverse of a spring constant, Eq. (3). The higher the value of k, the more volumetric strain for a given stress and hence a softer equivalent spring.

Factors with a significant effect on C are the percent moisture and particle size, when comparing <2- with <0.35-mm size fractions (Table 4). This is expected and logical. An increase in moisture content in the range 3–6 percent would be expected to increase the number of liquid bridge bonds between particles, and hence the overall cohesive stress (see Tschapek et al., 1985). Likewise, a reduction in particle size would reduce the effective pore size between the particles leading to increased capillary effects that would also increase C. It is interesting to note that C is not greatly affected by size, shape, orientation, or load order that suggests that the cohesive stresses

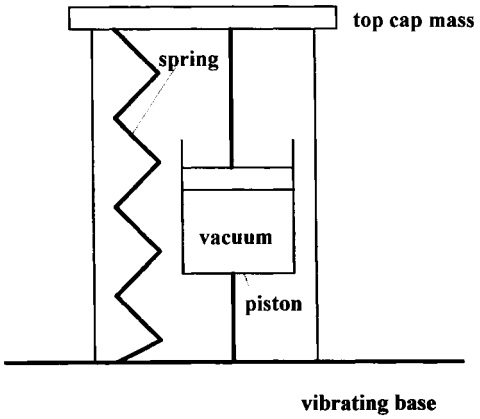

FIGURE 5 Spring and piston analogue for a bed of cohesive material.

in this material act isotropically. This is consistent with the liquid bridge bonding mechanism for cohesion and also conforms to the initial model assumptions concerning C, Eq. (5).

If the analogue shown in Fig. 5 behaved consistently, then changes in C would not affect the spring, merely the degree of compression. This is the case with particle size distribution, but not percent moisture, which is also a factor that affects k. Hence, there is an interaction between the mechanisms of elasticity and cohesion not included in the simple analogue.

Changes in k can be interpreted in terms of changes in the structure and nature of the particle bed. The bulk density is an obvious measure of bed structure that affects k. However, particle size distribution also affects bed structure, but this does not have a significant effect on k in these circumstances. This presents a paradox in the present set of data and further investigations are required. Sample shape, size, and percent moisture all have the potential to affect the packing of material in the bed. Sample shape and size affect the influence of die wall friction during the sample forming process. It is well-known that this affects compaction processes (Williams et al., 1970/71). Water may also act as a lubricant in the molds, enabling material to pack more readily. There is no evidence of structural asymmetry in these data, although other workers have reported such effects (Das, 1993). There are implications of the effects of sample size and shape on scale-up, and the data suggest that scale-up will not be a simple, linear process.

The presence of a membrane has a significant effect upon k, but not C. As far as the authors are aware, this is the first time that the effects of membrane containment have been investigated experimentally (Das, 1993). The particle bed is very stiff compared to the membrane, and the membrane should have a negligible effect. However, the membrane has been shown to have a definite effect and the membrane samples have a larger value of k than the freestanding ones. This is equivalent to a greater volumetric expansion for a given stress, or a softer spring equivalent, perhaps the reverse of what might be expected. It is standard procedure to test materials in soil mechanics in membrane enclosures. These data suggest that the contribution of membranes to such tests requires further investigation.

The significant effect of loading order suggests hysteresis in the elastic relationships, Eq. (3). This is consistent with observations in that Eq.

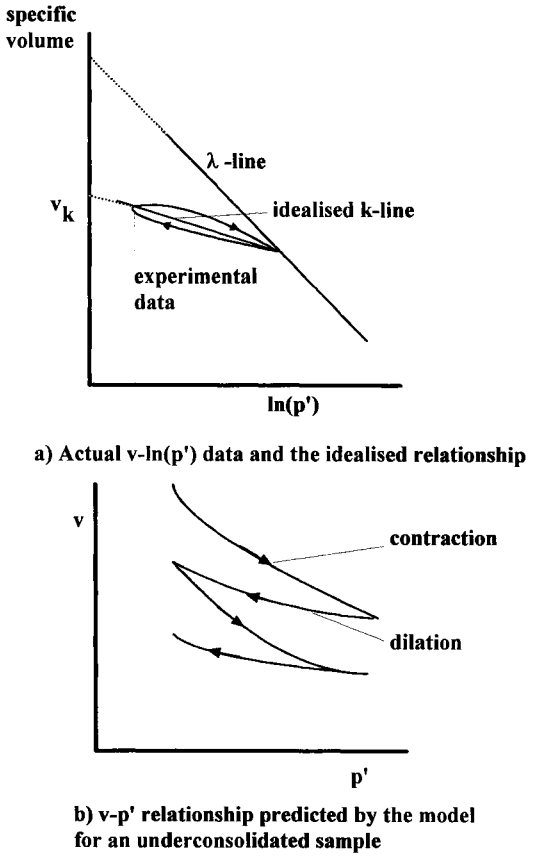

FIGURE 6 v versus $\ln(p')$ relationships: (a) showing hysteresis effects and (b) as predicted by the application of the model in the Appendix.

(3) is usually presented as a linearization of an elastic relationship with a degree of hysteresis [Schofield and Wroth, 1969; Fig. 6(a)].

The critical state model is subject to the assumptions inherent in the critical state theory of Schofield and Wroth (1969). In particular, it is assumed that the radial strain is equal to the axial strain during deformation. This allows the plastic deformation terms to be equal to zero in the energy balance equations of critical state theory that eliminates plastic flow from the model during elastic compression (see Appendix). This assumption is reasonable in certain types of triaxial tests where a sample is subjected to isotropic compression. However, the vibration tests shown in Fig. 1 impose an obvious imbalance of principal stresses: the axial stress changes during the vibration cycle, but the radial stresses remain constant. The Appendix shows the derivation of a modification to Eq. (4) to allow for a more general relationship between axial stress and radial stress, such that:

$$a_1 = \sqrt{\frac{3(1 + 2\alpha)p_s v_s}{WK_1 l_s}} \tag{9}$$

where a_1 is the natural frequency given by Eq. (9); α is the ratio of radial strain to axial strain, a negative form of the Poisson's ratio; and k_1 is the k line swelling constant given by Eq. (9).

When $\alpha = 1$, Eq. (9) becomes identical to Eq. (4) and $k_1 = k$. In terms of this more general model (Appendix), then

$$k = k_1(1 + 2\alpha)/3. \tag{10}$$

From the Appendix it is seen that the compression relation between v and $\ln(p')$ is different to the dilation relationship, Eq. (3) is replaced by two relationships, Eqs. (A.17)–(A.21) in the Appendix. If α is assumed to be a geometric factor governed by the packing, then as a first approximation, an underconsolidated sample will plastically compact through successive vibration cycles [Fig. 6(b)]. These changes are small and are not easily detectable, but may contribute to the effects of loading order on the results.

CONCLUSIONS

The transmission of sinusoidal vibration through beds of cohesive particulate solids was measured. Results were interpreted in terms of a critical state vibration model to predict the elastic swelling constant k, and the cohesive stress C.

Factorial experimental design has been used to identify significant parameters that affect k and C. Factors that affect k include percent moisture, bulk density, sample size, sample shape, the presence of a supporting membrane, and loading order. Factors affecting C include percent moisture and particle size distribution.

Results were explained in terms of changes in the structure of the particulate beds. An improved model was derived that explains the data.

This work was supported by a Cooperative Research grant, jointly sponsored by EPSRC and British Steel Technical, Teesside Laboratories, Middlesbrough, Cleveland, UK.

APPENDIX: MODEL OF SMALL AMPLITUDE, ELASTIC VIBRATION

This analysis follows closely that given by Matchett (1992). Consider the top cap mass (Fig. 1). There are three forces acting upon the mass:

1. the force of gravity;
2. the force due to the pressure of the environment, σ_r; and
3. the force due to axial stress in the material.

The equation of motion of the mass can be written, normalized to a unit area, assuming that changes in radius are negligible as

$$Wg + \sigma_r - \sigma_i = W\ddot{x} \tag{A.1}$$

where σ_r and σ_l are the radial and axial stresses, respectively. σ_r is zero in Fig. 1.

Assume that the material experiences a cohesion effect equivalent to a compressive stress C Pa. The effective consolidating stress p' can then be written as

$$p' = (2\sigma_r + \sigma_l)/3 + C \tag{A.2}$$

so

$$\sigma_l = 3p' - 2\sigma_r - 3C \tag{A.3}$$

and

$$v = v_k - k\ln(p')$$

or

$$p' = e^{\left(\frac{(v_k - v)}{k}\right)}. \tag{A.4}$$

Furthermore, under static conditions, the effective stress p_s and specific volume v_s are given by

$$p_s = \sigma_r + \frac{Wg}{3} + C \tag{A.5}$$

$$v_s = v_k - k\ln(p_s). \tag{A.6}$$

Equations (A.1)–(A.6) are given in the Matchett (1992) model. In that model, it was assumed that $de_l = de_r$, where de_l is the axial strain increment and de_r is the radial strain increment, with the convention that compressive strains and stresses are positive. This assumption eliminated plastic deformation from the model. Critical state theory for a Cam–Clay material is based upon an energy balance (Schofield and Wroth, 1969) of the following form (based upon a unit mass or unit volume of dry solids of initial volume v_o):

$$p'\left(\frac{dv}{v_o}\right) + qd\varepsilon - \left(\frac{k}{v_o}\right)dp' = Mp'|d\varepsilon| \tag{A.7}$$

where dv is the volumetric strain, $d\varepsilon$ is the shear strain, M is the critical state friction coefficient,

$$p' = (\sigma_l + 2\sigma_r)/3 + C\text{: } q = (\sigma_l - \sigma_r),$$

and

$$dv = v_o(de_l + 2de_r) \tag{A.8}$$

$$d\varepsilon = 2/3(de_l - de_r). \tag{A.9}$$

From Eqs. (A.7) and (A.9), when $de_l = de_r$, then $d\varepsilon$ is zero. The plastic, dissipative term disappears and the volumetric strain is elastic. This assumption is reasonable in a situation where axial stress and radial stress are equal, as in certain types of triaxial, soil mechanics tests. However, in the vibrational device shown in Fig. 1, this is not the case. Conventional linear elasticity theory assigns a Poisson ratio relating axial strain to radial strain. In these circumstances, it would be expected that compressive axial stress would result in an increase in radius, and although the Cam–Clay model is not linearly elastic, it may be assumed that over small strains the system approximates to such a state (Das, 1993).

Assume that there is a constant ratio between axial strain and radial strain, α, that is valid over the strains encountered. α may be positive or negative, but from the preceding arguments, α might be expected to be negative:

$$de_r = \alpha de_l. \tag{A.10}$$

From Eqs. (A.8), (A.9), and (A.10)

$$dv = (1 + 2\alpha)de_l$$

and

$$d\varepsilon = 2/3(1 - \alpha)de_l. \tag{A.11}$$

Equation (A.3) may be substituted into the equation of motion Eq. (A.1), and the resultant equations modified in terms of (A.4), (A.5), and (A.11), as in Matchett (1992). For small strains, the exponential relationship between p' and v [Eq. (A.4)] can be approximated to linearity to yield the ordinary differential equation:

$$\ddot{x} = -\frac{3(1 + 2\alpha)p_s v_s}{Wk_1 l_s}(x + y) \tag{A.12}$$

where y is the displacement of the base, and k_1 is the k value for the modified equation. Let

$$a_1^2 = \frac{3(1 + 2\alpha)}{Wk_1 l_s} p_s v_s \tag{A.13}$$

where a_1 is the natural frequency. Hence (A.12) becomes

$$\ddot{x} + a_1^2 x = -a_1^2 y. \tag{A.14}$$

The relationship between the original model and the modified model k values can be shown to be

$$k = \frac{k_1(1 + 2\alpha)}{3}.$$

k is the empirical swelling constant relating pressure to volume for compression under isotropic loading stresses and $\sigma_l = \sigma_r \cdot k_1$ represents a constant in the relationship when the loading is not symmetrical. An equivalent result can be obtained directly from the definitions of k, k_1, and geometric considerations.

It is an interesting footnote to substitute Eq. (A.11) into the critical state energy balance, Eq. (A.7). Considering a system of constant radial stress, σ_r is constant. Consider an underconsolidated sample such that $\alpha > -1/2$:

$$p'(1 + 2\alpha)de_l + 3(p' - (\sigma_r + C))2/3(1 - \alpha)de_l - kdp' = 2/3M(1 - \alpha)p'|de_l|. \tag{A.15}$$

Two cases can be considered:

$$\begin{aligned} &1.\ de_l < 0, \text{ when } |de_l| = -de_l \text{ and} \\ &2.\ de_l > 0, \text{ when } |de_l| = de_l. \end{aligned} \tag{A.16}$$

From (A.15) and (A.16), remembering that compressive strains are positive

$$dv(Ap' - B) = -kdp', \tag{A.17}$$

where

$$A = \left(\frac{9 \pm 2(1 - \alpha)M}{3(1 + 2\alpha)}\right) \tag{A.18}$$

and

$$B = \frac{2(1 - \alpha)(\sigma_r + C)}{(1 + 2\alpha)}. \tag{A.19}$$

Equation (A.18) uses the positive sign for $de_l < 0$ and the negative sign for $de_l > 0$.

Equation (17) may be integrated with the boundary condition:

$$p' = p_o : v = v_o \tag{A.20}$$

to give

$$v_o - v = \frac{k}{A} \ln \left(\frac{Ap' - B}{Ap_o - B} \right). \qquad \text{(A.21)}$$

Equation (A.21) gives a different form of pressure–volume relationship to the original equation, (A.4). This implies a change in volume with each vibration cycle, as the gradients of the compressive and dilation differ in $p' - v$ space (see [Fig. 6(b)]. Minor changes are also introduced into Eq. (A.12).

Unfortunately, it is very difficult to measure α with the small strains encountered in these tests. No significant data were obtained with a laser displacement transducer sensitive to 0.5 μm.

Similar arguments can be applied to overconsolidated samples, where it would be expected that the samples would dilate and therefore it would be expected that $\alpha < -1/2$.

REFERENCES

Das, B. M., 1993, *Principles of Soil Dynamics,* PWS-Kent Pub. Co., Boston.

Matchett, A. J., 1992, "Critical State Model for Vibration in Particulate Systems," *Powder Technology,* Vol. 70, pp. 63–70.

Norman–Gregory, G. M., and Selig, E. T., 1985, "Volume Change Behaviour of Vibrated Sand Columns," *Journal of Geotechnical,* Vol. 115, pp. 289–321.

Schofield, A., and Wroth, C. P., 1969, *Critical State Soil Mechanics,* McGraw–Hill, Reading, UK.

Thomson, W. T., 1981, *Theory of Vibration with Applications,* 2nd ed., Allen and Unwin, London, UK.

Tschapek, M., Falasca, S., and Wasowski, C., 1985, "The Undrained Water in Quartz Sand and Glass Beads," *Powder Technology,* Vol. 42, pp. 175–185.

Williams, J. C., Birks, A. H., and Bhattacherya, D., 1970/71, "The Direct Measurement of the Failure Function of a Cohesive Powder," *Powder Technology,* Vol. 4, pp. 328–337.

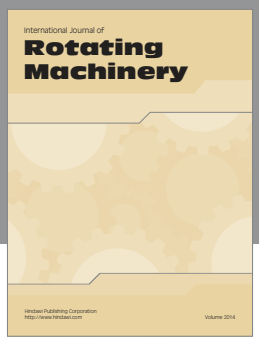

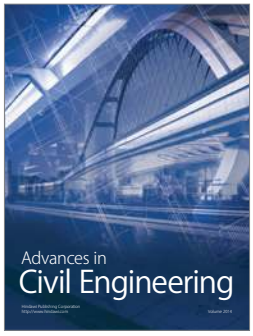

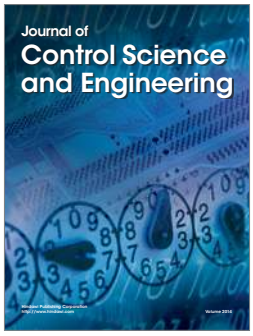

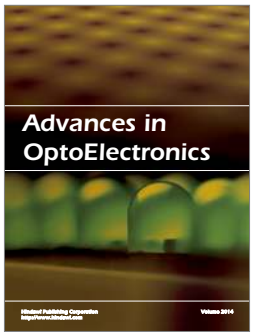

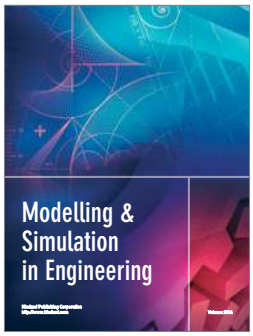

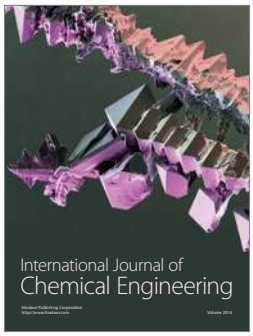

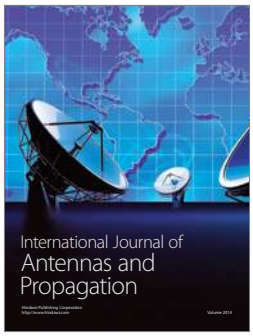

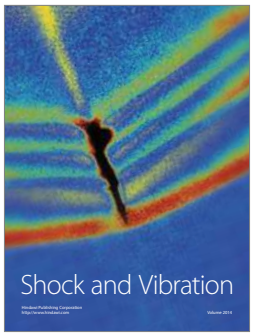

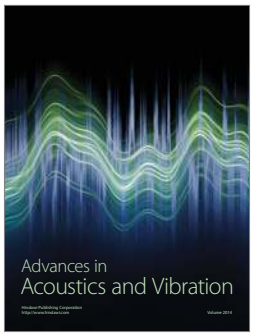

Hindawi

Submit your manuscripts at
http://www.hindawi.com